DOE/ET-53088-333 IFSR #333

Stability Thresholds of a Disk-Shaped Migma

H. Vernon Wong, M. N. Rosenbluth,
and *H. L. Berk*

Institute for Fusion Studies
The University of Texas at Austin
Austin, Texas 78712

August 1988

Stability Thresholds of a Disk-Shaped Migma

H. VERNON WONG, M. N. ROSENBLUTH,[a)]
and H. L. BERK
Institute for Fusion Studies
The University of Texas at Austin
Austin, Texas 78712

Abstract

The stability of a Migma disc is re-examined to determine the threshold to the interchange instability. It is shown that a previous calculation [H. L. Berk and H. V. Wong, Z. Naturforsch. **42a**, 1208 (1987)] which assumes a rigid mode eigenfunction, is inaccurate at the predicted particle number for marginal stability. As a result the integral equation for the system must be solved. A variational method of solution is developed and is shown to give good agreement with a direct numerical solution. The threshold for instability is found to be sensitive to the details of the distribution function. For highly focused systems, where all ions pass close to the axis, the threshold particle number (N_{u1}) for instability is substantially below that predicted by rigid mode theory ($N_{\rm rigid}$) (by a factor $\sim 8\epsilon^2$ where $\epsilon = r_1/r_L$, r_1 the spread in the distance of closest approach to the axis and r_L the ion Larmor radius). At a higher density a second band of stability appears that again destabilizes at yet higher particle number (N_{u2}). If $\epsilon \ll 1$, N_{u2} is substantially below the rigid mode prediction, while for $0.2 < \epsilon < 0.3$, N_{u2} is comparable to the rigid mode prediction. At moderate values

[a)]Present address: Univ. of California at San Diego, Dept. of Physics B-019, La Jolla, CA 92093

of $\epsilon(\epsilon \approx 0.3 - 0.4)$ the second stability band disappears and the instability particle number threshold varies from about $.4\epsilon$, when $\epsilon = 0.4$, to $.7\epsilon$ when ϵ is about unity. The stability criteria would be consistent with the observed particle storage number obtained in experimental configurations if the spread in ϵ is sufficiently large.

I. Introduction

The experimental establishment of a stable low-density $\left(\omega_{pi}^2/\omega_{ci}^2 \ll 1\right)$ Migma equilibrium configuration has been reported by D. Al Salameh et al.[1] A Migma equilibrium is a special type of axisymmetric mirror configuration in which the plasma is trapped in a disk-like volume centered at the mid-plane. Ideally, the ions are monoenergetic, their parallel velocity much less than the perpendicular velocity, and all the orbits pass through the axis of symmetry as indicated in Fig. 1.

In magnetohydrodynamic (MHD) theory, a symmetric mirror confined configuration is unstable to a flute interchange mode.[2] MHD stability criterion is altered by finite Larmor radius[3] and low density effects.[4,5] However, the analyses cited are deficient for a Migma configuration in that the Larmor radius is taken to be small compared to the plasma radius. More recently, Berk and Wong[6] have discussed the stability of Migma plasmas to $m = 1$ flute interchange instabilities in the limit of arbitrary particle Larmor radii. They concluded that the plasma response to a rigid mode $m = 1$ perturbation has a universal character independent of Larmor radius. As a result, the dispersion relation for flute interchange modes corresponding to rigid displacements is similar to that obtained by conventional finite Larmor radius theory. However, for a disk-shaped Migma equilibria (where the axial extent is much less than the plasma radius) the stability criteria was found to be more optimistic than previous investigations (5). The predicted particle number threshold N_{rigid} was above that achieved in the Migma experiment.

However, the Berk, Wong theory is inaccurate at densities near the predicted threshold for the onset of the $m = 1$ flute instability because the rigid mode approximation is not valid. The justification of the rigid mode approximation in their model requires the mode frequency to exceed the precessional frequency, whereas at marginal stability they found the real frequency is comparable to the precessional frequency. Thus a more accurate solution of the eigenmode equation is necessary to determine the instability thresholds.

In this paper, we construct a quadratic variational form from Poisson's equation for the perturbed electrostatic potential ϕ which is applicable to a disk-like plasma configuration. By choosing trial functions for ϕ which are localized in the regions of negative gradient in the plasma density, we obtain analytic instability criteria for ideal Migma configurations where the energetic ions all pass close to the axis of symmetry. Detailed numerical calculations confirm the results of the analytic procedure.

The results can be summarized as follows. Let $r_1/r_L = \epsilon$ define the radius r_1 within which the inner turning points of the ion orbits occur. r_L is the ion Larmor radius. For particle distributions with $\epsilon \ll 1$, two unstable particle number thresholds are found. At low particle number, there is an instability band where the threshold particle number N_{u1} for instability scales as ϵ^2 with stability reappearing at a higher particle number N_{s1}. For this instability band, the perturbations ϕ are localized near the inner turning points of the ion orbits where the plasma density gradient is negative. At yet a higher particle number N_{u2}, a second instability threshold occurs, with the perturbations localized at the plasma edge where the plasma density gradient is again negative. This unstable mode persists with increase in the particle number, eventually transforming into the rigid mode instability described in Ref. 6. For small values of $\epsilon \ll 1$, N_{u2} is below $N_{\rm rigid}$.

We have also investigated a configuration where conducting end plates surround the Migma configuration at distance d less than the particle Larmor radius, r_L. Similar stability criteria are obtained, but with the threshold particle storage number raised by a factor $\alpha r_L/d$ where α is roughly 0.5 .

The structure of the paper is as follows. In Sec. II we derive the dispersion relation for the system. In Sec. III the stability threshold is obtained using analytic procedures. Section IV discusses the stability criteria when conducting end plates are close to the Migma configuration. Section V compares the analytic method with a numerical solution using a series of Legendre polynomials. In Sec. VI, we summarize the principal results of our

investigation.

II. Quadratic Variational Form

The magnetic field is taken as a vacuum field which is approximately given by[7]

$$\mathbf{B} = \hat{\mathbf{z}} B_0 \left(1 + \frac{z^2}{L_m^2} - \frac{r^2}{2L_m^2}\right) - \hat{\mathbf{r}} B_0 \frac{rz}{L_m^2}. \tag{1}$$

The field line curvature is

$$\kappa \doteq \frac{1}{|B|}\frac{\partial |B|}{\partial r} = -\frac{r}{L_m^2}$$

and note that κ is second order in an expansion of $\epsilon \equiv r/L_m$.

We note that the particle motion can be obtained from gyro-orbit theory. It can be described as the gyration of a particle at the local cyclotron frequency about a guiding center position $\mathbf{r}_G$. As the axial extent of the particle's orbit is less than its radius, the guiding center radius can be taken as constant in the radial coordinate and the azimuthal guiding center angle, θ_G, rotates at the average rate

$$\bar{\dot{\theta}}_G \doteq \frac{\mu}{r\Omega_j}\frac{\partial |B|}{\partial r} = -\frac{\mu B_0}{\Omega_j L_m^2} \equiv \omega_{\kappa j} \tag{2}$$

Ω_j the cyclotron frequency $q_j B_0/m_j c$, m_j the particle mass,

$$\mu = \frac{v_\perp^2}{2\,|\mathbf{B}\,(\mathbf{r}_G)|} \equiv \text{magnetic moment.}$$

The guiding center position, which is axially focused by the mirror forces, is described by the equation

$$\frac{d^2 z}{dt^2} = -\mu \frac{\partial\,|B\,(r_G)|}{\partial z} = -2\mu \frac{B_0 z}{L_m^2}. \tag{3}$$

The solution for z is

$$z = z_0 \cos\left(\omega_z t + \beta_{z0}\right) \tag{4}$$

with $\omega_z^2 = 2\mu B_0/L_m^2$, $z_0 \equiv$ amplitude of the axial oscillation and β_z the axial phase. The axial adiabatic invariant $J_z = (2\pi)^{-1} \oint v_z dz$ is found to be

$$J_z = \frac{\omega_z z_0^2}{2} = \frac{1}{2}\omega_z \left(z^2 + \frac{v_z^2}{\omega_z^2}\right).$$

The actual radial position of the particle is shown in Fig. 2, where we have

$$\mathrm{r} = \mathrm{r}_G + \mathrm{r}_L,$$

which in component form can be expressed as

$$\begin{aligned} x &= r\cos\theta = r_G\cos\theta_G + r_L\cos\left(\beta_r + \theta_G\right) \\ y &= r\sin\theta = r_G\sin\theta_G + r_L\sin\left(\beta_r + \theta_G\right), \end{aligned} \tag{5}$$

where $\dot{\beta}_r = -\Omega_j$, and $r_L = (2\mu B_0)^{1/2}/\Omega_j$.

The average value of $\dot{\theta}_G$ has already been given, while the fluctuating value of $\dot{\theta}_G$ is small and can be neglected. Thus, we have $\theta_G = \theta_{G0} + \omega_\kappa \tau$.

The equilibrium distribution is a function of P_θ, μ, J_z, i.e.,

$$F = F\left(P_\theta, \mu, J_z\right), \tag{6}$$

where $P_\theta = rv_\theta + q_j\psi/m_j c \equiv$ canonical momentum per unit mass, and ψ is the magnetic flux function, which is given by

$$\psi = \frac{B_0 r^2}{2}\left(1 + \frac{z^2}{L_m^2}\right) + \mathcal{O}\left(\epsilon^2\right).$$

The phase space volume integral can be transformed to

$$d^3r\, d^3v = \frac{dJ_z\, d\mu\, dP_\theta\, dr\, dz\, d\theta |B| \omega_z}{|v_z|\ |v_r|} \tag{7}$$

with $v_r = \left[2\mu B - \left(P_\theta - q_j\psi/m_j c\right)^2/r^2\right]^{1/2}$ and $v_z = \omega_z\left[-z^2 + 2J_z/\omega_z\right]^{1/2}$.

The perturbed distribution, $f_j = \hat{f}_j \exp\left[-i\omega t + il\theta\right]$, satisfies the equation

$$\begin{aligned} \frac{Df_j}{Dt} &= \frac{q_j}{m_j}\nabla\phi \cdot \frac{\partial F}{\partial \mathrm{v}} \\ &= \frac{q_j}{m_j}\left[il\phi\frac{\partial F}{\partial P_\theta} + \frac{\mathrm{v}_\perp \cdot \nabla\phi}{|B|}\frac{\partial F}{\partial \mu} + \frac{v_z}{\omega_z}\frac{\partial \phi}{\partial z}\frac{\partial F}{\partial J_z}\right], \end{aligned} \tag{8}$$

where D/Dt denotes the convective derivative over unperturbed orbits and $\phi(\mathbf{r},t) = \hat{\phi}(r,z)\exp[-i\omega t + il\theta]$. Now $\mathbf{v}_\perp \cdot \nabla\phi = D\phi/Dt + i\omega\phi - v_z\partial\phi/\partial z$. Then integrating in time yields

$$\begin{aligned} \hat{f}_j &= \frac{q_j}{m_j}\frac{\hat{\phi}}{B}\frac{\partial F}{\partial \mu} + \frac{q_j}{m_j}\int_{-\infty}^{0} d\tau \exp\left[-i\omega\tau + il\left(\theta(\tau)-\theta\right)\right] \\ &\quad \times\left[il\hat{\phi}\left(r(\tau),z(\tau)\right)\frac{\partial F}{\partial P_\theta} + v_z\frac{\partial\hat{\phi}}{\partial z}\frac{1}{\omega_z}\frac{\partial F}{\partial J_z} + \left(i\omega - v_z\frac{\partial}{\partial z}\right)\frac{\hat{\phi}}{B}\frac{\partial F}{\partial\mu}\right], \end{aligned} \tag{9}$$

where $\theta(\tau)$ is the azimuthal angle over the unperturbed orbit with $\theta(\tau) = \theta$ at $\tau = 0$.

We now expand the periodic orbit $\hat{\phi}(r,z)/r$ in a double Fourier time series

$$\frac{\hat{\phi}\left(r(\tau),z(\tau)\right)}{r(\tau)} = \sum_{m,n}\exp\left[im\left(\omega_z\tau + \beta_{z0}\right) + in\left(-\bar{\Omega}\tau + \beta_{r0}\right)\right]\left(\frac{\hat{\phi}}{r}\right)_{m,n} \tag{10}$$

with

$$\left(\frac{\hat{\phi}}{r}\right)_{m,n} \doteq \frac{\omega_z}{2\pi}\int_0^{2\pi/\omega_z} dt\frac{\phi\left(r(t),z(t)\right)}{r}\exp\left[in\left(\bar{\Omega}t - \beta_{r0}\right) - im\left(\omega_z t + \beta_{z0}\right)\right], \tag{11}$$

where $\bar{\Omega}$ is the mean cyclotron frequency averaged over an axial bounce (as the mean cyclotron frequency is nearly the same as the local cyclotron frequency we will equate the two frequencies; we have also ignored small orbital sideband terms that arise due to the difference between the mean and local cyclotron frequencies and used that $\omega_z \ll \Omega$). Note that it is readily shown that

$$\left(\frac{\hat{\phi}}{r}\right)_{m,n} = \left(\frac{\hat{\phi}}{r}\right)_{m,-n}.$$

We now limit our study to the $l = 1$ mode and use from Eq. (5)

$$\begin{aligned} r(\tau)\exp\left[i\left(\theta(\tau)-\theta\right)\right] &= (x+iy)e^{-i\theta} \\ &= \left[r_G + r_L\cos\left(-\Omega\tau + \beta_{r0}\right) + ir_L\sin\left(-\Omega\tau + \beta_{r0}\right)\right] \\ &\quad \cdot\exp\left[i\omega_\kappa\tau + i\theta_{g0} - i\theta\right]. \end{aligned} \tag{12}$$

We now delete the caret on $\hat{\phi}$ and $\hat{f}_j$. For simplicity we will not exhibit the ion behavior to the $v_z\partial\phi/\partial z$ term since it is complicated and ultimately unimportant in our application.

The electron contribution from the $v_z\partial\phi/\partial z$ term is more important than the ion term. We shall observe that the electron response to the $v_z\partial\phi/\partial z$ term allows for a flute perturbation in which $\partial\phi/\partial z$ is negligible in the region where ions and electrons are contained. Thus the complicated $\partial\phi/\partial z$ ion term will not appear in the final result.

We now perform the τ integration and we obtain for ions ($j = i$) to lowest order in ω/Ω_i and ω/ω_z,

$$\begin{aligned} f_i &= \frac{q_i}{m_i}\frac{\phi}{B}\frac{\partial F}{\partial \mu} \\ &- \frac{q_i}{m_i}\frac{\exp\left[-i\left(\theta-\theta_{g0}\right)\right]}{\omega-\omega_\kappa}\left(\frac{\partial F}{\partial P_\theta}+\frac{\omega}{B}\frac{\partial F}{\partial \mu}\right)\left[r_G\left(\frac{\phi}{r}\right)_{0,0}+\frac{r_{Li}}{2}\left(\left(\frac{\phi}{r}\right)_{0,1}+\left(\frac{\phi}{r}\right)_{0,-1}\right)\right] \\ &+ \theta\left(\frac{\omega}{\Omega_i}\right)+\theta\left(\frac{\omega}{\omega_z}\right)+\left(\frac{\partial\phi}{\partial z}\quad\text{terms}\right). \end{aligned} \tag{13}$$

For electrons we neglect FLR terms so that $\phi_{n,m} = \phi_m\delta_{n,0}$, we assume $\omega \gg \omega_{\kappa e}$ and we find

$$f_e = -\frac{q_e}{\omega m_e}\frac{\partial F_e}{\partial P_\theta}\phi_0+\frac{q_e}{m_e\omega_z}\left(\phi(r,z)-\phi_0\right)\frac{\partial F}{\partial J_z}, \tag{14}$$

where

$$\phi_0 = \frac{\pi}{\omega_z}\int_{-z_T}^{z_T}\frac{dz}{v_z}\phi(r,z)$$

with $v_z\left(r,\pm z_T\right)=0$.

We can now substitute f_j given by Eqs. (13) and (14) into Poisson's Equation

$$\nabla^2\left(\phi e^{i\theta}\right) = -4\pi\sum_j e^{i\theta}q_j\int d^3v\, f_j. \tag{15}$$

We then form a quadratic form by multiplying by $\phi^+ = \phi(r,z)\exp\left(-i\theta\right)$, and integrating over all space. Assuming ϕ decays at infinity, and neglecting boundary effects, we obtain

$$L(\phi,\phi) \equiv \int\frac{d^3r}{4\pi}\nabla\phi^+\cdot\nabla\left(\phi e^{i\theta}\right)-\sum_j q_j\int d^3r\, d^3v\,\phi^+e^{i\theta}f_j$$

$$= \int \frac{d^3r}{4\pi}\left[\left(\frac{\partial\phi}{\partial r}\right)^2+\left(\frac{\partial\phi}{\partial z}\right)^2+\frac{\phi^2}{r^2}\right]-\frac{q_i^2}{m_i}\left\langle\frac{\partial F_i}{B\partial\mu}\phi^2-\frac{I_1^2(\phi)\left(\frac{\partial F_i}{\partial P_\theta}+\frac{\omega}{B}\frac{\partial F_i}{\partial\mu}\right)}{\omega-\omega_{\kappa i}}\right\rangle$$

$$-\frac{q_e^2}{m_e}\left\langle\left(\phi^2-\phi_0^2\right)\frac{1}{\omega_z}\frac{\partial F_e}{\partial J_z}-\frac{\phi_0^2}{\omega}\frac{\partial F_e}{\partial P_\theta}\right\rangle=0, \tag{16}$$

where $\langle\ \ \rangle$ denotes a six-dimensional phase space integration and

$$I_1(\phi)=\frac{\omega_z\Omega_i}{\pi^2}\int_{-z_T}^{z_T}\frac{dz}{|v_z|}\int_{r_{\min}}^{r_{\max}}\frac{\phi(r,z)}{r}\left[r_G+r_L\cos\Omega_i\tau\right]\frac{dr}{v_r}, \tag{17}$$

where $r_{\min}$ and $r_{\max}$ are the limits of the radial variation of r. We also note that for ions in Migma,

$$\omega\frac{\partial F_i}{\partial\mu}\Big/\frac{\partial F_i}{\partial P_\theta}\approx\frac{\omega}{\Omega_i},$$

and hence we can neglect all $\partial F_i/\partial\mu$ terms.

Due to the small axial length of the plasma disk compared to the plasma radius, $Z_T \ll r_0$, the dominant terms in the quadratic form if $\varphi(z)$ can vary cover the scale length Z_T, is

$$\int_{-Z_T}^{Z_T}\frac{dz}{4\pi}\left(\frac{\partial\phi}{\partial z}\right)^2-\frac{q_e^2}{m_e}\left\langle\left(\phi^2-\phi_0^2\right)\frac{1}{\omega_Z}\frac{\partial F_e}{\partial J_Z}\right\rangle.$$

The $|\nabla_\perp\phi|^2$ terms, with $|\nabla_\perp\phi|\sim\phi/r_0$, are clearly much less that $(\partial\phi/\partial z)^2$, and we ultimately seek solutions where the remaining terms are comparable to $|\nabla_\perp\phi|^2$ terms. Thus, to annihilate the lowest order quadratic term, we need to consider flute modes where $\phi=\phi_0$. The remaining terms of the quadratic form require that then ϕ inside the plasma disk be constrained to a flute structure.

The ratio of the second term to the first term is Z_T^2/λ_{De}^2, where the electron Debye length is

$$\lambda_{De}=\left(\frac{T_e}{4\pi N_e e^2}\right)^{1/2}$$

(N_e is the equilibrium electron density and T_e the electron temperature). If $Z_T^2/\lambda_{De}^2\gg 1$, the justification for flute modes is even stronger, with validity of the flute mode assumption requiring

$$\frac{1}{r_0}<\frac{1}{Z_T}+\frac{1}{\lambda_{De}}.$$

We assume that there are no equilibrium electric fields so the $q_e N_e = -q_i N_i$. We then use

$$\begin{aligned}\left\langle \frac{q_e^2}{m_e}\frac{\partial F_e}{\partial P_\theta}\frac{\phi^2}{\omega}\right\rangle &= \frac{q_e}{\omega}c\int d^3r\frac{\partial N_e}{\partial\psi}\phi^2 \\ &= -\frac{q_i c}{\omega}\int d^3r\frac{\partial N_i}{\partial\psi}\phi^2 \\ &= -\frac{cq_i}{\omega}\int d^3r\,\phi^2\frac{\partial}{\partial\psi}\int d^3v\,F_i.\end{aligned}$$

Now as

$$F_i\left(P_\theta,\mu,J_z\right) = F_i\left(rv_\theta+\frac{q_i\psi}{m_i c},\frac{v_\perp^2}{2B},\frac{v_z^2+z^2}{2\omega_z}\right)$$

we find that

$$\frac{\partial}{\partial\psi}\int d^3v\,F = \frac{q_i}{m_i c}\int d^3v\frac{\partial F}{\partial P_\theta}\left[1+\frac{\dot\theta}{\Omega_i}\right]+\mathcal{O}(\kappa r).$$

One can ascertain that

$$\frac{\dot\theta}{\Omega_i} = -\frac{r_L^2 - r_L r_G\cos\beta_r}{r^2}$$

and $r^2 = r_G^2 + r_L^2 + 2r_L r_G\cos\beta_r$. Consequently we find

$$\left\langle \frac{q_e^2}{m_e}\frac{\partial F_e}{\partial P_\theta}\frac{\phi^2}{\omega}\right\rangle = -\frac{q_i c}{\omega}\int d^3r\frac{\partial N_i}{\partial\psi}\phi^2 = -\left\langle \frac{q_i^2}{m_i}\frac{\partial F_i}{\partial P_\theta}\frac{I_2}{\omega}\right\rangle, \tag{18}$$

where

$$I_2 = \frac{\Omega_i}{2\pi}\oint d\tau\frac{\phi^2\left(r(\tau)\right)}{r^2(\tau)}\left\{r_G^2+r_G r_L\cos\Omega_i\tau\right\}. \tag{19}$$

Equation (18) allows the remaining electron term in the quadratic form (Eq. (16)) to be expressed in terms of the ion distribution function.

There remains to be evaluated the contribution of the electric field energy integrated over all space. We use the identity

$$\int d^3r\,\nabla\phi\cdot\nabla\phi^+ = 4\pi\int d^3r\,\rho\phi,$$

where $4\pi\rho = -\nabla^2\phi$ and we have assumed $\phi \to 0$ at external boundaries. As we have a thin disc, the predominant contribution of the left-hand integral comes from the vacuum region with an error $\mathcal{O}(z_T/r_L)$. To this approximation the electric field in the vacuum can be viewed as due to a surface charge $\rho(r,z) = \sigma(r)\delta(z)$. Then to determine ϕ in the vacuum outside the plasma, we note that

$$\phi(r,z) = \int \frac{d^3r'\sigma(r')\delta(z')e^{i(\theta'-\theta)}}{[(z-z')^2 + r^2 + r'^2 - 2rr'\cos(\theta'-\theta)]^{1/2}}. \tag{20}$$

Since $\phi(r,z) = \phi(r)$ at $z = 0$

$$\phi(r) = \int_0^{r_0} r'dr' \int_0^{2\pi} d\zeta \frac{\sigma(r')\cos\zeta}{[r^2 + r'^2 - 2rr'\cos\zeta]^{1/2}}.$$

If we convert the integration in ζ to a contour integration in $R \equiv rr'e^{i\zeta}$ around a circle of radius rr' encircling the branch points at $R = 0$ and $R = \min(r'^2, r^2)$, and we deform this contour along the real axis, we obtain (with $s^2 = \mathrm{Re}\, R$)

$$\begin{aligned}\phi(r) &= \frac{4}{r}\int_0^{r_0} dr'\sigma(r') \int_0^{\min(r,r')} ds \frac{s^2}{[(r^2-s^2)(r'^2-s^2)]^{1/2}} \\ &= \frac{4}{r}\int_0^{r} ds \frac{s^2}{(r^2-s^2)^{1/2}} \int_s^{r_0} \frac{dr'\sigma(r')}{(r'^2-s^2)^{1/2}}.\end{aligned} \tag{21}$$

Let

$$W(s) = \int_s^{r_0} \frac{dr'\sigma(r')}{(r'^2-s^2)^{1/2}}.$$

By Abel inversion

$$\begin{aligned}sW(s) &= \frac{1}{2\pi}\int_0^s ds' \frac{1}{(s^2-s'^2)^{1/2}} \frac{\partial s'\phi(s')}{\partial s'} \\ \sigma(r) &= -\frac{2}{\pi}\frac{\partial}{\partial r}\int_r^{r_0} ds \frac{sW(s)}{(s^2-r^2)^{1/2}}\end{aligned}$$

$$r_0 > r > r.$$

Thus

$$\frac{1}{4\pi}\int d^3r\, \nabla\left(\phi^+ e^{-i\theta}\right)\cdot\nabla\left(\phi e^{i\theta}\right) = \int d^3r\, \rho\phi e^{-i\theta}$$

$$= -4\int_0^{r_0} dr\, r\phi(r)\frac{\partial}{\partial r}\int_r^{r_0}\frac{ds\, sW(s)}{(s^2-r^2)^{1/2}}$$

$$= 8\pi\int_0^{r_0} dr\,\{rW(r)\}^2\,. \tag{22}$$

The quadratic variational form may now be written as follows:

$$L(\phi,\phi) = \frac{2}{\pi}\int_0^{r_0} dr\left\{\int_0^r ds\frac{1}{(r^2-s^2)^{1/2}}\frac{\partial}{\partial s}s\phi(s)\right\}^2$$

$$- \left\langle\frac{q_i^2}{m_i}\frac{\partial F_{0i}}{\partial P_\theta}\frac{I_2}{\omega}\right\rangle + \left\langle\frac{q_i^2}{m_i}\frac{\partial F_{0i}}{\partial P_\theta}\frac{I_1^2}{(\omega-\omega_\kappa)}\right\rangle = 0. \tag{23}$$

If we model the ion distribution function by an ideal Migma configuration

$$F_i\left(P_\theta,\mu,J_z\right) = \frac{\Omega_i N_T\delta\left(\mu B_0 - \mu_0 B_0\right) f_0\left(P_\theta\right) f_1\left(J_z\right)}{(2\pi)^3\int dJ_z f_1\left(J_z\right)\int dP_\theta f_0\left(P_\theta\right)} \tag{24}$$

the quadratic form simplifies to

$$\frac{\pi}{2r_0}L(\phi,\phi) = L_1(\phi,\phi) - \frac{\lambda}{\hat{\omega}}L_2(\phi,\phi) + \frac{\lambda}{\hat{\omega}-1}L_3(\phi,\phi) = 0, \tag{25}$$

where

$$L_1(\phi,\phi) \equiv \int_0^1 d\xi\left\{\int_0^\xi\frac{d\xi'}{(\xi^2-\xi'^2)^{1/2}}\frac{\partial}{\partial\xi'}\xi'\phi(\xi')\right\}^2, \tag{26}$$

$$L_2(\phi,\phi) \equiv -\int dp\frac{\partial f_0}{\partial p}\frac{r_0^2}{r_L^2}I_2, \tag{27}$$

$$L_3(\phi,\phi) \equiv -\int dp\frac{\partial f_0}{\partial p}\frac{r_0^2}{r_L^2}I_1^2, \tag{28}$$

where $f_1\left(J_z\right)$ is sharply peaked about $J_z = 0$, N_T is the total number of ions, and

$$\lambda \equiv \frac{\pi q_i^2 N_T}{2m_i\Omega_i r_0^3\left|\omega_\kappa\right|}$$

$$p \equiv \frac{P_\theta}{\Omega_i r_L^2}$$

$$\int dp f_0(p) = 1$$

$$
\begin{aligned}
\omega_\kappa &= -\frac{\mu_0 B_0}{\Omega_i L_m^2} \\
\hat{\omega} &= \frac{\omega}{\omega_\kappa} \\
\xi &= \frac{r}{r_0} \\
r_L^2 &= \frac{2\mu_0 B_0}{\Omega_i^2} \\
r_G^2 &= r_L^2 + \frac{2P_\theta}{\Omega_i} \\
r_0 &= \left[r_G\left(p = p_{\max}\right) + r_L\right] \\
&= r_L\left[(1 + 2p_{\max})^{1/2} + 1\right] \equiv \text{plasma radius.}
\end{aligned}
$$

The requirement that the first variation of the quadratic form with respect to ϕ be stationary yields the eigenvalue equation which must be solved to determine $\hat{\omega}$.

In the limit of large $\lambda \gg 1$, the quadratic form to lowest order is

$$
L \approx -\frac{\lambda}{\hat{\omega}} \int dp \frac{\partial f_0}{\partial p} \left(I_2 - I_1^2\right) \frac{r_0^2}{r_L^2}. \tag{29}
$$

By the Schwartz inequality,

$$
I_2 - I_1^2 = r_G^2 \left[\left(\int_0^1 du\right)\left(\int_0^1 du \frac{\phi^2}{r^2}\right) - \left(\int_0^1 du \frac{\phi}{r}\right)^2\right] \geq 0,
$$

where

$$
du = \frac{(r_G + r_L \cos\tau)}{2\pi r_G} d\tau.
$$

Thus L is stationary to lowest order when $I_2 - I_1^2$ is minimized to zero. This occurs for the trial function

$$
\phi = \frac{r}{r_0}
$$

which corresponds to the "rigid" mode approximation discussed in Ref. 6. In this case, the perturbed electric field amplitude is independent of radius r, and the electron and ion

drifts due to the perturbed electric field are the same, independent of the Larmor radius. Substituting for ϕ in Eqs. (26)–(28) yields

$$\begin{aligned} L_1 &= \frac{4}{3} \\ I_1 &= \frac{r_G}{r_0} = \frac{r_L}{r_0}(1+2p)^{1/2} \\ I_2 &= \frac{r_G^2}{r_0^2} \\ L_2 &= 2 \\ L_3 &= 2. \end{aligned}$$

The dispersion relation obtained from Eq. (25) is then

$$\frac{2\lambda}{\hat{\omega}(\hat{\omega}-1)} + \frac{4}{3} = 0. \tag{30}$$

The frequency $\hat{\omega}$ is

$$\hat{\omega} = \frac{1}{2}\left[1 \pm (1-6\lambda)^{1/2}\right] \approx \pm i\left(\frac{3}{2}\lambda\right)^{1/2},$$

where $\lambda \gg 1$ is required for validity. Thus, the equilibrium is unstable to rigid mode perturbation at large values of $\lambda \gg \lambda_{\text{rigid}} = 1/6$, that is,

$$N_T \gg N_{\text{rigid}} \equiv \frac{m_i r_0^3 \Omega_i \left|\omega_\kappa\right|}{3\pi q_i^2} \approx \frac{8 m_i r_L^3 \Omega_i \left|\omega_\kappa\right|}{3\pi q_i^2}. \tag{31}$$

However, at the threshold for the onset of the instability, the rigid mode approximation is no longer valid. A more accurate solution of the eigenmode equations is necessary to determine the instability thresholds.

If we formally solve Eq. (25) for $\hat{\omega}$, we obtain

$$\hat{\omega} = \frac{1}{2L_1}\left\{\lambda\left(L_2 - L_3\right) + L_1 \pm G^{1/2}\right\}, \tag{32}$$

where

$$G \equiv (\lambda(L_2 - L_3) + L_1)^2 - 4\lambda L_1 L_2$$

$$= (\lambda(L_2 - L_3) - L_1)^2 - 4\lambda L_1 L_3.$$

Since L_1 is positive definite, necessary conditions for instability are $L_2 > 0$, $L_3 > 0$. L_2 is positive if ϕ is nonzero only in the range of r where

$$\frac{\partial N_i}{\partial \psi} < 0.$$

If we restrict the class of trial functions to that for which $L_2 > 0$, $L_3 > 0$

$$G = \left[\lambda\left(L_2^{1/2} + L_3^{1/2}\right)^2 - L_1\right]\left[\lambda\left(L_2^{1/2} - L_3^{1/2}\right)^2 - L_1\right] \tag{33}$$

and hence $G < 0$ and the equilibrium is unstable if the value of λ is in the range

$$\lambda_s > \lambda > \lambda_u,$$

where

$$\lambda_u = \frac{L_1}{\left(L_2^{1/2} + L_3^{1/2}\right)^2} \tag{34}$$

$$\lambda_s = \frac{L_1}{\left(L_2^{1/2} - L_3^{1/2}\right)^2}. \tag{35}$$

In order to explore these thresholds, we investigate two simple representative examples of the distribution function $f_0(p)$, and we obtain approximate dispersion relations by substitution of simple trial functions in the quadratic form.

III. Instability Threshold

A. Simple trial functions

Let us consider a rectangular distribution function

$$f_0(p) = \frac{1}{(p^+ - p^-)}, \qquad p^+ > p > p^-$$

$$f_0(p) = 0, \qquad \text{otherwise.} \tag{36}$$

To further simplify the analysis, let

$$p^- = -\epsilon\left(1-\frac{\epsilon}{2}\right)$$
$$p^+ = \epsilon\left(1+\frac{\epsilon}{2}\right).$$

Thus

$$\frac{r_G(p^+)}{r_L} = 1+\epsilon$$
$$\frac{r_G(p^-)}{r_L} = 1-\epsilon.$$

The inner turning point of all the energetic ions (encircling and noncircling) are within a radius less than $r_1 = r_G(p^+) - r_L = r_L - r_G(p^-) = \epsilon r_L$. The outermost turning points for ions which do and do not encircle the axis of symmetry occur at $r_2 \equiv r_G(p^-) + r_L = (2-\epsilon)r_L$ and $r_0 \equiv r_G(p^+) + r_L = (2+\epsilon)r_L$, respectively.

The equilibrium density integrated over z is

$$n_i = \frac{2B_0(2\pi)}{r}\int \frac{dJ_z\, d\mu\, dP_\theta F_i(P_\theta,\mu,J_z)}{|v_r|}$$
$$= \frac{N_T}{(p^+-p^-)\,2\pi^2 r_L}\int_{p^-}^{p^+}\frac{dp\,\theta\left[r^2-(pr_L-r^2/2r_L)^2\right]}{\left[r^2-(pr_L-r^2/2r_L)^2\right]^{1/2}}$$

with $\theta(x)$ a step function. Performing the integration, we obtain

$$n_i = \begin{cases} n_0, & r_1 > r \\ \frac{n_0}{\pi}\left[\sin^{-1}\frac{r_0}{2r_L}\left(\frac{r_1}{r}-\frac{r}{r_0}\right)+\sin^{-1}\frac{r_2}{2r_L}\left(\frac{r_1}{r}+\frac{r}{r_2}\right)\right], & r_2 > r > r_1 \\ \frac{n_0}{\pi}\left[\sin^{-1}\frac{r_0}{2r_L}\left(\frac{r_1}{r}-\frac{r}{r_0}\right)+\frac{\pi}{2}\right], & r_0 > r > r_2 \end{cases} \quad (37)$$

with $n_0 = N_T/4\epsilon r_L^2\pi$. At $r = r_1,\ r_0$, $\partial n_i/\partial r \to -\infty$, while at $r = r_2$, $\partial n_i/\partial r \to \infty$. For $\epsilon \ll 1$, $n_i(r=r_2)/n_0 \approx (2\epsilon)^{1/2}/\pi$. In Fig. 3, we plot $n_i(r)/n_0$ as a function of r.

A. Let us first consider a trial function which is localized at the inner radius $r = r_1$

$$\phi(r) = \begin{cases} r/r_0 & r_1 > r \\ r_1^2/r_0 r & r > r_1. \end{cases} \quad (38)$$

The maximum of $\phi(r)$ is placed at $r = r_1$ in order to weight preferentially the region of negative $\partial n_i/\partial\psi$, thereby maximizing L_2. We confirm later that this trial function is close to an eigenfunction of the eigenmode equation.

Substituting for ϕ in Eqs. (26), (27), and (28), we obtain

$$L_1 = \frac{8}{3}\xi_1^3 + 4\left\{\frac{2}{3} - \xi_1^2 - \frac{2}{3}\left(1-\xi_1^2\right)^{3/2}\right\} \tag{39}$$

$$\xi_1 = \frac{r_1}{r_0} = \frac{\epsilon}{2+\epsilon}$$

$$I_2\left(p^+\right) = \left.\frac{r_1^4 r_G^2}{r_0^2\left(r_G^2 - r_L^2\right)^2}\right|_{p=p^+} = \frac{\epsilon^2(1+\epsilon)^2}{(2+\epsilon)^2}\frac{r_L^2}{r_0^2} \tag{40}$$

$$I_2\left(p^-\right) = \left.-\frac{r_1^4 r_G^2}{r_0^2\left(r_L^2 - r_G^2\right)^2}\right|_{p=p^-} = -\frac{\epsilon^2(1-\epsilon)^2}{(2-\epsilon)^2}\frac{r_L^2}{r_0^2} \tag{41}$$

$$I_1\left(p^+\right) = \left.\frac{r_1^2}{r_G r_0}\right|_{p=p^+} = \frac{\epsilon^2}{(1+\epsilon)}\frac{r_L}{r_0} \tag{42}$$

$$I_1\left(p^-\right) = 0 \tag{43}$$

$$L_2 = \frac{1}{2\epsilon}\left[\frac{r_0^2}{r_L^2}I_2\right]_{p^-}^{p^+} = \frac{\epsilon\left(4 - 3\epsilon^2 + \epsilon^4\right)}{\left(4-\epsilon^2\right)^2} \tag{44}$$

$$L_3 = \frac{1}{2\epsilon}\left[\frac{r_0^2}{r_L^2}I_1^2\right]_{p^-}^{p^+} = \frac{\epsilon^3}{2(1+\epsilon)^2}. \tag{45}$$

The frequency of the modes approximated by this trial function is determined by Eq. (32). When $\lambda \to 0$, there are two modes with $\hat{\omega}$ real; one mode $\hat{\omega} \approx 1$ at the precessional frequency of the ions, and the other $\hat{\omega} \approx \lambda L_2/L_1$ proportional to λ involving the electrons. As λ increases, the modes approach each other in frequency, and eventually they couple resonantly, resulting in an instability.

$\hat{\omega}$ has complex solutions and the equilibrium is unstable if λ lies in the range

$$\lambda_{s1} > \lambda > \lambda_{u1},$$

where λ_{u1} and λ_{s1} are determined by Eqs. (34) and (35), respectively

$$\bar{\lambda}_{u1} = \frac{\lambda_{u1}}{\lambda_{\text{rigid}}} = \frac{8}{(2+\epsilon)^3} \frac{\left\{16+24\epsilon+6\epsilon^2+\epsilon^3-16(1+\epsilon)^{3/2}\right\}}{\left\{\left[\frac{\epsilon\left(4-3\epsilon^2+\epsilon^4\right)}{\left(4-\epsilon^2\right)^2}\right]^{1/2}+\left[\frac{\epsilon^3}{2(1+\epsilon)^2}\right]^{1/2}\right\}^2}$$

$$\approx 8\epsilon^2 \qquad \epsilon \ll 1.$$

This trial function approximates an eigenfunction at the instability threshold λ_{u1} but not at the stability threshold λ_{s1}. However, the existence of the stability threshold λ_{s1} has been confirmed by using a more complex trial function for ϕ and by representing ϕ as a sum over a set of Legendre polynomials.

In Table I, we tabulate the values of $\bar{\lambda}_{u1}$ from the above formula for a range of ϵ varying from .01 to 1.0 .

B. Let us next consider a trial function which is a maximum at the plasma edge $r = r_0$:

$$\phi(r) = \frac{r_1}{r_0}\left(1-\frac{r_1}{r}\right), \qquad r_0 > r > r_1. \tag{46}$$

Substituting for ϕ in Eqs. (26), (27), and (28)

$$L_1 = \xi_1^2 \int_{\xi_1}^1 d\xi \left\{\frac{\pi}{2} - \sin^{-1}\frac{\xi_1}{\xi}\right\}^2$$

$$= \xi_1^2\left[\left(\frac{\pi}{2}-\theta_1\right)^2 + \pi\xi_1 \ln\tan\frac{\theta_1}{2} + 2\xi_1\int_{\theta_1}^{\pi/2} d\theta \frac{\theta}{\sin\theta}\right], \tag{47}$$

where $\sin\theta_1 = \xi_1$.

$$I_2\left(p^+\right) = \left\{\frac{r_1^4}{r_0^2}\frac{r_G^2}{\left(r_G^2-r_L^2\right)^2} + \frac{r_1^2}{r_0^2}\right.$$

$$\left. - \frac{2r_1^3}{\pi r_0^2\left(r_G+r_L\right)}\left[\frac{\left(r_G-r_L\right)E\left(\kappa^2\right)}{\left(r_G+r_L\right)\left(1-\kappa^2\right)} + K\left(\kappa^2\right)\right]\right\}_{p+} \tag{48}$$

$$I_2\left(p^-\right) = \left\{-\frac{r_1^4}{r_0^2}\frac{r_G^2}{\left(r_L^2-r_G^2\right)^2}\right.$$

$$- \frac{2r_1^3}{\pi r_0^2 (r_G + r_L)} \left[\frac{(r_G - r_L) E(\kappa^2)}{(r_G + r_L)(1 - \kappa^2)} + K(\kappa^2) \right] \Bigg\}_{p^-} \quad (49)$$

$$I_1(p^+) = \left\{ \frac{r_1^2}{r_0 r_G} - \frac{r}{\pi r_0 r_G} \left[(r_G - r_L) K(\kappa^2) + (r_G + r_L) E(\kappa^2) \right] \right\}_{p^+} \quad (50)$$

$$I_1(p^-) = -\left\{ \frac{r_1}{\pi r_0 r_G} \left[(r_G - r_L) K(\kappa^2) + (r_G + r_L) E(\kappa^2) \right] \right\}_{p^-} \quad (51)$$

$$L_2 = \frac{1}{2\epsilon} \frac{r_0^2}{r_L^2} \left\{ I_2(p^+) - I_2(p^-) \right\} \quad (52)$$

$$L_3 = \frac{1}{2\epsilon} \frac{r_0^2}{r_L^2} \left\{ I_1^2(p^+) - I_1^2(p^-) \right\}, \quad (53)$$

where $K(k^2)$ and $E(k^2)$ are the complete elliptic integrals of the first and second kind:

$$K(k^2) = \int_0^{\pi/2} d\theta \frac{1}{\left[1 - k^2 \sin^2\theta\right]^{1/2}}$$

$$E(k^2) = \int_0^{\pi/2} d\theta \left[1 - k^2 \sin^2\theta\right]^{1/2}$$

and

$$k^2 \equiv \frac{4 r_G r_L}{(r_G + r_L)^2}.$$

The dispersion relation is similar to that described in the previous section, and it again predicts a range of λ within which the equilibria is unstable. However, this trial function approximates an eigenfunction only at the instability threshold $\lambda = \lambda_{u2}$ where λ_{u2} is determined by Eq. (34), and no evidence of a second stability threshold $\lambda = \lambda_{s2}$ was found using a more complex trial function for ϕ or by representing ϕ as a sum over a set of Legendre polynomials.

For $\epsilon \ll 1$,

$$L_1 \approx \frac{\pi^2}{16} \epsilon^2 \quad (54)$$

$$L_2 = \frac{1}{2\epsilon} \frac{r_0^2}{r_L^2} \left\{ I_2(p^+) - I_2(p^-) \right\} \approx \frac{\epsilon}{4\pi} (3\pi - 8) \quad (55)$$

$$L_3 = \frac{1}{2\epsilon} \frac{r_0^2}{r_L^2} \left\{ I_1^2(p^+) - I_1^2(p^-) \right\} \approx \frac{4\epsilon^2}{\pi^2} \left(\ln \frac{8}{\epsilon} - 1 - \frac{\pi}{2} \right) \quad (56)$$

and the instability threshold λ_{u2} is

$$\begin{aligned}\bar{\lambda}_{u2} &= \frac{\lambda_{u2}}{\lambda_{\text{rigid}}} = 6\lambda_{u2} \\ &= \frac{3\pi^3\epsilon}{2(3\pi-8)\left\{1+4\left[\frac{\epsilon}{\pi}\frac{(\ln 8/\epsilon - 1 - \pi/2)}{3\pi-8}\right]^{1/2}\right\}^2}. \end{aligned} \tag{57}$$

In Table II, we tabulate the values of $\bar{\lambda}_{u2}$ for a range of ϵ varying from 0.0001 to 0.3.

C. Let us now consider a more complex trial function which can represent modes peaked at either r_1 or at r_0

$$\phi(r) = \begin{cases} a_1 \frac{r}{r_0}, & r_1 > r \\ \frac{r_1}{r_0}\left\{(a_1+a_2)\frac{r_1}{r} - a_2\right\}, & r_2 > r > r_1 \\ \frac{r_1}{r_0}\left\{(a_1+a_2)\frac{r_1}{r} - a_2\right\} + a_3\frac{(r-r_2)}{r_0}, & r_0 > r > r_2. \end{cases} \tag{58}$$

a_1, a_2, and a_3 are variational parameters. This trial function is essentially a 2-parameter trial function since the third is a normalization constant.

Substituting for ϕ in Eqs. (26), (27), and (28)

$$\begin{aligned} L_1 &= \int_0^{\xi_1} d\xi 4a_1^2\xi^2 + \int_{\xi_1}^{\xi_2} d\xi \left\{2a_1\left(\xi - \left(\xi^2-\xi_1^2\right)^{1/2}\right) - a_2\xi_1\left(\frac{\pi}{2} - \sin^{-1}\frac{\xi_1}{\xi}\right)\right\}^2 \\ &+ \int_{\xi_2}^{1} d\xi \left\{2a_1\left(\xi - \left(\xi^2-\xi_1^2\right)^{1/2}\right) - a_2\xi_1\left(\frac{\pi}{2} - \sin^{-1}\frac{\xi_1}{\xi}\right)\right. \\ &+ \left. a_3\left(2\left(\xi^2-\xi_2^2\right)^{1/2} - \xi_2\left(\frac{\pi}{2} - \sin^{-1}\frac{\xi_2}{\xi}\right)\right)\right\}^2 \end{aligned} \tag{59}$$

$$\begin{aligned} I_2\left(p^+\right) &= \frac{\Omega_i}{2\pi}\oint d\tau \frac{(r_G^2 + r_G r_L\cos\Omega_i\tau)}{r_0^2}\left\{(a_1+a_2)\frac{r_1^2}{r^2} - a_2\frac{r_1}{r}\right\}^2\Big|_{p^+} \\ &+ \frac{\Omega_i}{\pi}\int_0^{\tau_2} d\tau \frac{(r_G^2 + r_G r_L\cos\Omega_i\tau)}{r_0^2}\left\{2a_3\left(1-\frac{r_2}{r}\right)\left((a_1+a_2)\frac{r_1^2}{r^2} - a_2\frac{r_1}{r}\right)\right. \\ &+ \left. a_3^2\left(1-\frac{r_2}{r}\right)^2\right\}_{p^+} \end{aligned} \tag{60}$$

$$I_1\left(p^-\right) = \frac{\Omega_i}{2\pi}\oint d\tau \frac{(r_G^2 + r_G r_L\cos\Omega_i\tau)}{r_0^2}\left\{(a_1+a_2)\frac{r_1^2}{r^2} - a_2\frac{r_1}{r}\right\}^2\Big|_{p^-} \tag{61}$$

$$I_1\left(p^+\right) = \frac{\Omega_i}{2\pi}\oint d\tau \frac{\left(r_G + r_L\cos\Omega_i\tau\right)}{r_0}\left\{\left(a_1+a_2\right)\frac{r_1^2}{r^2} - a_2\frac{r_1}{r}\right\}\Big|_{p^+}$$
$$+ \frac{\Omega_i}{\pi}\int_0^{\tau_2} d\tau \frac{\left(r_G + r_L\cos\Omega_i\tau\right)}{r_0} a_3\left(1-\frac{r_2}{r}\right)\Big|_{p^+} \tag{62}$$

$$I_1\left(p^-\right) = \frac{\Omega_i}{\pi}\oint \frac{d\tau}{2\pi} \frac{\left(r_G + r_L\cos\Omega_i\tau\right)}{r_0}\left\{\left(a_1+a_2\right)\frac{r_1^2}{r^2} - a_2\frac{r_1}{r}\right\}_{p^-} \tag{63}$$

$$L_2 = \frac{1}{2\epsilon}\frac{r_0^2}{r_L^2}\left\{I_2\left(p^+\right) - I_2\left(p^-\right)\right\} \tag{64}$$

$$L_3 = \frac{1}{2\epsilon}\frac{r_0^2}{r_L^2}\left\{I_1^2\left(p^+\right) - I_1^2\left(p^-\right)\right\}, \tag{65}$$

where

$$\xi_1 = \frac{r_1}{r_0}, \qquad \xi_2 = \frac{r_2}{r_0}$$
$$r^2 = r_G^2 + r_L^2 + 2r_G r_L\cos\Omega_i\tau$$

and τ_2 is determined by

$$\frac{r_2^2}{r_L^2} = \frac{1}{r_L^2}\left(r_G^2 + r_L^2 + 2r_G r_L\cos\Omega_i\tau_2\right)\Big|_{p^+}.$$

Equation (25) can therefore be written as the following matrix equation

$$\sum_{n,n'=1}^{3}\alpha_{n'}\left\{B_{n',n} - \Lambda C_{n',n}\right\}\alpha_n = 0, \tag{66}$$

where $B_{n',n}$ and $C_{n',n}$ are defined by

$$\sum_{n,n'=1}^{3}\alpha_{n'}C_{n',n}\alpha_n \equiv L_1 \tag{67}$$

$$\sum_{n,n'=1}^{3}\alpha_{n'}B_{n',n}\alpha_n \equiv -\hat{\omega}L_3 + (\hat{\omega}-1)L_2 \tag{68}$$

and

$$\Lambda = \frac{\hat{\omega}(\hat{\omega}-1)}{\lambda}$$

$$\alpha_1 = a_1 + a_2$$

$$\alpha_2 = a_2$$

$$\alpha_3 = a_3.$$

This quadratic form is stationary with respect to variation of α_n if

$$\sum_{n'=1}^{3} \{B_{n',n} - \Lambda C_{n',n}\} \alpha_n = 0$$

$$n = 1, 2, 3 \tag{69}$$

and nontrivial solutions of this system of homogeneous equations exist if the determinant of the coefficients α_n is zero

$$D(\hat{\omega}, \lambda) = |B_{n',n} - \Lambda C_{n',n}| = 0. \tag{70}$$

The three eigenvalues $\Lambda^{(j)}$ of this equation for $\hat{\omega}$ real have been determined numerically. In Fig. 4, we plot the solutions for

$$\lambda^{(j)} = \frac{\hat{\omega}(\hat{\omega} - 1)}{\Lambda^{(j)}(\hat{\omega})}$$

of real $\hat{\omega}$ for $\epsilon = 0.2$. One of the eigenvalues $\Lambda^{(2)}(\hat{\omega})$ is zero at $\hat{\omega} = 1$, and hence $\lambda^{(2)}$ is finite at $\hat{\omega} = 1$.

Let λ_{u1} be the value of λ at which

$$\frac{\partial \lambda^{(1)}}{\partial \hat{\omega}} = 0,$$

and let λ_{u2}, λ_{s1} $(\lambda_{u2} > \lambda_{s1})$ be the values of λ at which

$$\frac{\partial \lambda^{(2)}}{\partial \hat{\omega}} = 0.$$

At low values of $\lambda < \lambda_{u1}$, all the roots of $\hat{\omega}$ are real and the plasma equilibrium is stable. At higher values $\lambda_{s1} > \lambda > \lambda_{u1}$, two roots of $\hat{\omega}$ are complex and an unstable mode exists. When $\epsilon \ll 1$, this mode is peaked at the inner radius r_1 and has a radial profile similar to the trial function discussed in (a). It becomes stable if $\lambda > \lambda_{s1}$.

At large values of $\lambda > \lambda_{u2}$, a second mode becomes unstable. When $\epsilon \ll 1$, this mode is peaked at the plasma edge and has a radial profile similar to the trial function discussed in (b). At even larger values of λ, this mode transforms into the rigid mode perturbation.

In Fig. 5, we plot the trial functions $\varphi_u^{(1)}$, $\varphi_s^{(2)}$, $\varphi_u^{(2)}$ corresponding to the eigenvalues $\lambda^{(1)} = \lambda_{u1}$, $\lambda^{(2)} = \lambda_{s1}$, $\lambda^{(2)} = \lambda_{u2}$, respectively.

In Table III, we tabulate the values of $\bar{\lambda}_{u1} = \lambda_{u1}/\lambda_{\rm rigid}$, $\bar{\lambda}_{s1} = \lambda_{s1}/\lambda_{\rm rigid}$, and $\bar{\lambda}_{u2} = \lambda_{u2}/\lambda_{\rm rigid}$ for a range of ϵ varying from 0.01 to 1.0. For $\epsilon \ll 1$, the thresholds $\bar{\lambda}_{u1}$, $\bar{\lambda}_{u2}$ predicted using the simpler trial functions discussed in (a) and (b) (see Table I and Table II) are close to those listed in Table III. When $\epsilon > 0.4$, the stable band disappears.

In Fig. 6, we delineate the regions of stability and instability by plotting $\bar{\lambda}_{u1}$, $\bar{\lambda}_{s1}$, and $\bar{\lambda}_{u2}$ as a function of ϵ.

IV. End Plates

The presence of conducting end plates located at $z = \pm d$ on either side of the disk-shaped plasma can readily be included in the theory when $d \ll r_0$. In this limit, the perturbed Laplace equation for the perturbed potential ϕ between the plates is approximately $\partial^2\phi/\partial z^2 = 0$, so that the solution for ϕ is

$$\phi = \begin{cases} \phi(r)\frac{(d-z)}{d}e^{i\theta}, & d > z > 0 \\ \phi(r)\frac{(z+d)}{d}e^{i\theta}, & 0 > z > -d. \end{cases}$$

Therefore the contribution to the quadratic variational form of the perturbed fields in the vacuum is

$$\frac{1}{4\pi}\int d^3r\, \nabla\phi^+ \cdot \nabla\phi \approx \frac{1}{d}\int_0^{r_0} dr\, r\phi^2(r).$$

In the rigid mode approximation where $\phi(r) = r/r_0$, we obtain for the quadratic term $L_1(\phi,\phi)$

$$L_1 = \frac{\pi r_0}{8d}$$

and the rigid mode dispersion relation determined by Eq. (25) is

$$\hat{\omega}(\hat{\omega} - 1) = -\frac{2\lambda}{L_1} = -8\hat{\lambda},$$

where $\hat{\lambda} = 2d\lambda/r_0$. The mode is unstable if $32\hat{\lambda} > 1$, corresponding to a particle number threshold $(N_{\rm rigid})_{\rm end\ plate}$ for onset of the instability

$$(N_{\rm rigid})_{\rm end\ plate} = \frac{3\pi r_L}{16d} N_{\rm rigid}.$$

Thus a close end plate offers the possibility of storing more particles than the isolated system treated previously.

To consider stability to nonrigid perturbations we substitute the trial function defined by Eq. (58) for $\phi(r)$, we obtain for the quadratic term $L_1(\phi,\phi)$

$$\begin{aligned} L_1 \;=\; & \frac{\pi r_0}{2d}\Bigg[(a_1+a_2)^2 \xi_1^4 \left(\frac{1}{4} - \log\xi_1\right) - (a_1+a_2)\, a_2 \xi_1^3 \left(2 - 3\frac{\xi_1}{2}\right) + a_2^2 \xi_1^2 \left(\frac{1}{2} - \frac{\xi_1^2}{4}\right) \\ & + a_3^2 \left(\frac{1}{4} - 2\frac{\xi_2}{3} + \frac{\xi_2^3}{2} - \frac{\xi_2^4}{12}\right) + a_3 (a_1+a_2)\, \xi_1^2 (1-\xi_2)^2 - a_3 a_2 \xi_1 \left(\frac{2}{3} - \xi_2 + \frac{\xi_2^3}{3}\right) \Bigg]. \end{aligned}$$

We may now repeat the calculation described in Sec. IIIC to determine the eigenvalues

$$\hat{\lambda}(\hat{\omega}) \equiv \frac{2d}{\pi r_0}\lambda(\hat{\omega})$$

and thereby obtain the thresholds for stability and instability. The structure of the stability boundaries are unchanged, and in Table IV, we tabulate the values of

$$\bar{\hat{\lambda}}_{u1} = \frac{\hat{\lambda}_{u1}}{\hat{\lambda}_{\rm rigid}}, \quad \bar{\hat{\lambda}}_{s1} = \frac{\hat{\lambda}_{s1}}{\hat{\lambda}_{\rm rigid}}, \quad \bar{\hat{\lambda}}_{u2} = \frac{\hat{\lambda}_{s2}}{\hat{\lambda}_{\rm rigid}}$$

for a range of values of ϵ.

Note that the use of end plates introduces significant enhancements of the particle number thresholds only when the end plate separation is small enough to satisfy the inequality $d/r_L < 3\pi/16$.

V. Instability Threshold (Legendre Polynomial Representation)

In order to obtain more accurate results and to extend the investigation to other distribution functions, we have represented ϕ as a sum over a set of Legendre polynomials in $\xi = r/r_0$,

derived the equivalent matrix quadratic form, and solved the resulting matrix eigenvalue equation numerically. Let

$$\int_0^\xi d\xi' \frac{1}{(\xi^2-\xi'^2)^{1/2}} \frac{\partial}{\partial \xi'} \xi' \phi(\xi') = \sum_{n=0}^{\infty} a_n (4n+3)^{1/2} P_{2n+1}(\xi)$$

$$1 \geq \xi \geq 0, \tag{71}$$

where $P_{2n+1}(\xi)$ are Legendre polynomials of order $2n+1$.

By Abel inversion, we obtain for $\phi(\xi)$

$$\begin{aligned} \phi(\xi) &= \sum_{n=0} a_n \frac{(4n+3)^{1/2}}{\pi \xi} \int_0^\xi d\xi' \frac{2\xi' P_{2n+1}}{(\xi^2-\xi'^2)^{1/2}} \\ &= \sum_{n=0} a_n \sum_{m=0}^{n} b(n,m) \xi^{2n+1-2m}, \end{aligned} \tag{72}$$

where

$$b(n,m) \equiv \frac{(-1)^m (4n+3)^{1/2}}{2^{2n+1}} \begin{pmatrix} 2n+1 \\ m \end{pmatrix} \begin{pmatrix} 4n+2-2m \\ 2n+1 \end{pmatrix} \begin{pmatrix} n-m+1/2 \\ -1/2 \end{pmatrix}$$

$$\begin{pmatrix} 2n+1 \\ m \end{pmatrix} \equiv \frac{\Gamma(2n+2)}{\Gamma(m+1)\Gamma(2n+2-m)}$$

and $\Gamma(m+1)$ is the Gamma-function.

Substituting Eq. (72), for ϕ in Eqs. (26)–(28)

$$L_1 = \sum_{n,m=0}^{\infty} a_n \delta_{n,m} a_m \tag{73}$$

$$I_2 = \frac{r_G r_L}{r_0^2} \sum_{n,m=0}^{\infty} a_n a_m \sum_{n'=0}^{n} \sum_{m'=0}^{m} b(n,n') b(m,m') Q_{n-n'+m-m'} \tag{74}$$

$$I_1 = \frac{r_L}{r_0} \sum_{n=0}^{\infty} a_n \sum_{n'=0}^{n} b(n,n') Q_{n-n'} \tag{75}$$

$$L_2 = -\int dp \frac{\partial f_0}{\partial p} \frac{r_0^2}{r_L^2} I_2 \tag{76}$$

$$L_3 = -\int dp \frac{\partial f_0}{\partial p} \frac{r_0^2}{r_L^2} I_1^2, \tag{77}$$

where

$$
\begin{aligned}
Q_l &= \frac{\Omega_i}{2\pi}\oint d\tau \left(\frac{r_G}{r_L}+\cos\Omega_i\tau\right)\left\{\frac{1}{r_0^2}\left(r_G^2+r_L^2+2r_Gr_L\cos\Omega_i\tau\right)\right\}^l \\
&= \left(\frac{r_G+r_L}{r_0}\right)^{2l}\left\{\left(\frac{r_G}{r_L}+1\right)F\left(\frac{1}{2},-l;1;k^2\right)-F\left(\frac{3}{2},-l;2;k^2\right)\right\} \\
&= \left(\frac{r_G+r_L}{r_0}\right)^{2l}\frac{\Gamma(l+1/2)}{\Gamma(1/2)\Gamma(l+1)}k^{-4}\Bigg[\left(\frac{r_G}{r_L}+1\right)F\left(\frac{1}{2},\frac{1}{2};\frac{1}{2}-n;1-\frac{1}{k^2}\right) \\
&\qquad -\frac{k^{-2}}{(n+1)}F\left(\frac{3}{2},\frac{1}{2};\frac{1}{2}-n;1-\frac{1}{k^2}\right)\Bigg], \qquad (78)
\end{aligned}
$$

where

$$k^2=\frac{4r_Gr_L}{(r_G+r_L)^2},$$

and $F(1/2,-l,1;k^2)$ is the hypergeometric function.

Equation (23) can be written as the following equivalent matrix equation

$$\sum_{n,m} a_n\left\{M_{n,m}-\Lambda\delta_{n,m}\right\}a_m=0, \qquad (79)$$

where

$$a_nM_{n,m}a_m = (\hat{\omega}-1)L_2-\hat{\omega}L_3 \qquad (80)$$

$$\Lambda = \frac{\hat{\omega}(\hat{\omega}-1)}{\lambda}. \qquad (81)$$

This quadratic form is stationary with respect to variations of a_n if

$$\sum_{m=0}\left(M_{n,m}-\Lambda\delta_{n,m}\right)a_m=0$$

$$n=0,1,\ldots \qquad (82)$$

and nontrivial solutions of this system of homogeneous equations exist if the determinant of the coefficients is zero

$$D(\hat{\omega},\lambda)=\left|M_{n,m}-\Lambda\delta_{n,m}\right|=0. \qquad (83)$$

The matrix elements $M_{n,m}$ were evaluated numerically using:

1. a rectangular distribution function $f(p)$ (Eq. (36));

2. a parabolic distribution function $f(p)$:

$$f(p) = \frac{3}{4p_0}\left[1 - \frac{(p-\bar{p})^2}{p_0^2}\right], \qquad |p-\bar{p}| \leq p_0. \tag{84}$$

$\bar{p}$ determines the position of the maximum and p_0 the width of the distribution function.

For purposes of comparison with the square distribution function, it should be noted that the inner turning points for ions which do (do not) encircle the axis of symmetry are within a radius less than $r_1^-\left(r_1^+\right)$, where

$$\begin{aligned} r_1^- &= r_L - r_G\left(p = -p_0\right) = \epsilon^- r_L \\ r_1^+ &= r_G\left(p = p_0\right) - r_L = \epsilon^+ r_L \end{aligned}$$

and

$$\begin{aligned} \epsilon^- &= 1 - (1 - 2p_0)^{1/2} \\ \epsilon^+ &= (1 + 2p_0)^{1/2} - 1. \end{aligned}$$

For a given order matrix $M_{n,m}(\hat{\omega})$, with $\hat{\omega}$ real, the eigenvalues $\Lambda^{(j)}$ are determined numerically. The order of the matrix is increased until the roots of interest, namely the lowest roots algebraically, have converged. By plotting

$$\lambda^{(j)} = \frac{\hat{\omega}(\hat{\omega}-1)}{\Lambda^j(\hat{\omega})}$$

as a function of $\hat{\omega}$, we can determine the values of λ at which $\partial\lambda^{(j)}/\partial\hat{\omega} = 0$, and thereby obtain the stability thresholds $\bar{\lambda}_{u1}$, $\bar{\lambda}_{s1}$, and $\bar{\lambda}_{u2}$ identified in Sec. III using simple trial functions.

In Table V, we tabulate the values of $\bar{\lambda}_{u1}$, $\bar{\lambda}_{s1}$, and $\bar{\lambda}_{u2}$ obtained for a rectangular distribution function $f_0(p)$ (see Eq. (36)) identical to that considered in the previous section. The magnitude of ϵ ranges from $\epsilon = 0.2$ to 1.0.

When $\epsilon < 0.2$, the roots did not converge for a finite number of Legendre polynomials $n \leq 14$. Numerical inaccuracies begin to appear when $n > 14$, and no acceptable solutions could be determined for small values of $\epsilon < 0.2$.

Over the range of ϵ where convergence could be ascertained, the results for $\bar{\lambda}_{u1}$, $\bar{\lambda}_{s1}$, and $\bar{\lambda}_{u2}$ are similar to those listed in Table III. They confirm the adequacy of the simple trial function used in Section III.

In order to explore the sensitivity of the results to the particle distribution function, we repeated the above calculation for a parabolic distribution function $f(p)$. The structure of the boundary curves separating the stable and unstable regions remained the same. The corresponding results for the stability thresholds for differing values of p_0 are listed in Table VI.

VI. Discussion

The assumption of a rigid mode approximation simplifies considerably the analysis of the flute instability in Migma equilibrium configuration. The particle number threshold N_{rigid} for onset of the flute instability was determined to be

$$N_{\text{rigid}} = \frac{8 m_i r_L^3 \Omega_i \, |\omega_\kappa|}{3\pi q_i^2} \equiv \frac{4 m_i r_L^5 \Omega_i^2}{3\pi L_m^2 q_i^2},$$

where $r_0 \approx 2 r_L$.

However, the rigid mode approximation can be justified only when the mode frequency is larger than the ion precessional frequency. At marginal stability, the real frequency is comparable to the precessional frequency, and thus a more accurate solution of the eigenmode equation is necessary to determine the instability thresholds. This was accomplished by substitution of a two-parameter trial function for the perturbed potential $\phi(r)$ in a quadratic variational form constructed from Poisson's equation. The accuracy of these results was confirmed by solving the eigenmode equation with $\phi(r)$ represented as a sum over a set of Legendre polynomials.

For a nearly ideal Migma equilibria, where $\epsilon = r_1/r_L \ll 1$ (r_1 is the inner turning point of the ion orbit), two unstable particle number thresholds were found.

The first instability threshold for the particle number N_{u1} scales as

$$\frac{N_{u1}}{N_{\text{rigid}}} = 8\epsilon^2$$

if $\epsilon \ll 1$, with stability appearing at a higher particle number N_{s1}. In this instability band, $N_{s1} > N_T > N_{u1}$, the unstable perturbations are localized near the inner negative density gradient.

At yet a higher particle number N_{u2}

$$\frac{N_{u2}}{N_{\text{rigid}}} = \frac{3\pi^3\epsilon}{2(3\pi-8)\left\{1+4\left[\frac{\epsilon}{\pi}\frac{(\ln 8/\epsilon - 1 - \pi/2)}{3\pi-8}\right]^{1/2}\right\}^2}$$

a second instability threshold occurs, with the unstable perturbations localized at the edge. With further increases in the particle number this unstable mode eventually transforms into the rigid mode instability.

Figure 6 displays the boundaries between the stable and unstable regions in the parameter space of N_T/N_{rigid} versus ϵ. When $\epsilon > .4$, the stable band disappears.

When conducting end plates are present at a distance d on either side of the disk-shaped plasma, the enhancement of the particle number thresholds become significant only when $d/r_L < 3\pi/16$, where $2d$ is the plate separation distance and r_0 the disk-plasma radius.

We note that our stability condition may give a plausible explanation of stability regimes achieved in the Migma experiment. In the experiment reported in Ref. 1 a 600 KeV deuterium plasma was prepared in a 3 Tesla magnetic field where $\omega_\kappa/\omega_{ci} = 0.039$ and that a particle storage number of 3×10^{11} was achieved. The calculated value of N_{rigid} is 1.1×10^{12} particles. In Ref. 1 the radial spread of orbits is reported as 0.4 cm and we note that the gyroradius is ~ 5 cm so that $\epsilon \approx 0.1$. Thus, $N_T/N_{\text{rigid}} \approx .3$ was stable. In Fig. 6 we see that $N_T/N_{\text{rigid}} \approx .3$ and $\epsilon \approx 0.1$ is in the second stability region. It was further reported that the particle

storage number was achieved after passing through noisy regimes at lower particle storage number. These noisy regimes occur both as particle storage number increases and decreases at particle storage values that are roughly independent of the increasing or decreasing phase. In Ref. 1 the band of noisy behavior occurs between 0.3 and 0.5 of the maximum achieved particle storage number. This behavior suggests that in the experiment the plasma may be passing through the unstable band predicted in our theory both in its increasing particle storage phase and decreasing storage phase. Note that at $\epsilon = 0.1$ our theory predicts an instability band for particle storage numbers between 0.16 and 0.5 of the observed maximum achieved particle storage numbers. This correlates qualitatively with experiment. Our theory has neglected the effects of equilibrium electric fields that may exist, as well as an offset in the P_θ distribution (Ref. 1 indicates that the mean P_θ in the experiment is shifted from zero). Further, the plasma should respond to the noisy regime by spreading radially. These uncertainties make more quantitative comparisons of experiment and theory difficult. Nonetheless, some evidence of the instability band is indicated in the experimental results.

Other explanations of the noisy phase of the observed experimental results also need to be considered. It has been suggested by Maglich[7] that the noisy phase of Migma operation is due to the loss of axial focusing of a non-neutral positively charged plasma that arises as the ion storage builds up. This effect may be relevant during the phase where particle storage increases. During the decreasing particle storage phase, it is more difficult to understand why an already charge neutral system should have trouble with axial focusing.

Yet other possible explanations for the noisy intervals may be relevant. Maglich[7] has pointed out the importance of coupling of axial electron motion to the ion cyclotron frequency. He notes that higher particle storage is obtained only when the axial electron bounce frequency exceeds the ion cyclotron frequency. Our theory does not describe this effect. We however note that such an effect may be an indication of a loss cone type mode[8–10] where ion cyclotron effects interact with axial electron dynamics. One should also note that

nonlinear effects can complicate mode identification. For example, it is possible that charge imbalance caused by an unstable flute mode could induce electron bounce-mode excitations.

Finally we note that our theory indicates that the experiment has achieved a particle storage level that is still below the critical level for the second instability band.

If we assume $\epsilon = 0.1$, we expect another unstable regime to arise when N exceeds 7×10^{11} particles for an experiment with otherwise the same parameters as reported in Ref. 1. This second instability threshold is of more global nature than the first instability regime (in the latter case the perturbation is localized near the origin), and may give rise to a significant limitation on the particle number that can be stored. Further experiments are needed to test the validity of our theoretical predictions.

Acknowledgements

This research was supported by U. S. Dept. of Energy Contract No. DE-FG05-80ET-53088. We would like to thank Dr. B. Maglich for his encouragement and useful comments.

References

1. D. Al Salameh, S. Channon, B. R. Cheo, R. Leverton, B. C. Maglich, S. Menasian, R. A. Miller, J. Nering, and C. Y. Wu, Phys. Rev. Letters **54**, 796 (1985).

2. M. N. Rosenbluth and C. L. Longmire, Annals of Phys. **1**, 120 (1957).

3. M. N. Rosenbluth, N. A. Krall, and N. Rostoker, Nuc. Fus. Suppl. Pt. 1, 143 (1962).

4. C. C. Damm, J. H. Foote, A. H. Futch, Jr., A. L. Gardner, F. J. Gordon, A. L. Hurt, and R. F. Post, Phys. Fluids **8**, 1472 (1965).

5. N. A. Krall, Phys. Fluids **9**, 820 (1966).

6. H. L. Berk and H. V. Wong, Z. Naturforsch. **42a**, 1208 (1987).

7. B. Maglich, Nuclear Instruments and Methods in Physics Research A271, 13–36 (1988).

8. E. G. Harris, Phys. Rev. Lett. **2**, 34 (1959).

9. M. N. Rosenbluth and R. F. Post, Phys. Fluids **8**, 547 (1965).

10. W. M. Sharp, H. L. Berk, and C. E. Nielsen, Phys. Fluids **22**, 1975 (1979).

ϵ	$\bar{\lambda}_{u1}$
.01	.00077
.05	.0161
.1	.0534
.2	.53
.3	.260
.4	.362
.5	.455
.6	.539
.7	.613
.8	.677
.9	.727
1.0	.760

Table I. Tabulation of $\bar{\lambda}_{u1}$—rectangular distribution function $f_0(p)$ and trial function Eq. (38).

ϵ	$\bar{\lambda}_{u2}$
.0001	.0029
.001	.0245
.01	.163
.05	.485
.1	.705
.2	.938
.3	1.04

Table II. Tabulation $\bar{\lambda}_{u2}$—rectangular distribution function $f_0(p)$ and trial function Eq. (46).

ϵ	$\bar{\lambda}_{u1}$	$\bar{\lambda}_{s1}$	$\bar{\lambda}_{u2}$
.01	.00076	.0023	.147
.05	.016	.049	.42
.1	.053	.17	.62
.2	.15	.53	.88
.3	.26	.92	1.08
.4	.36	1.24	1.25
.5	.45		
.6	.53		
.8	.66		
1.0	.73		

Table III. Tabulation of $\bar{\lambda}_{u1}$, $\bar{\lambda}_{s1}$, $\bar{\lambda}_{u2}$—rectangular distribution function $f_0(p)$ and trial function Eq. (58).

ϵ	$\bar{\bar{\lambda}}_{u1}$	$\bar{\bar{\lambda}}_{s1}$	$\bar{\bar{\lambda}}_{u2}$
.1	.011	.032	.204
.2	.050	.163	.436
.3	.111	.369	.644
.4	.185	.602	.818
.5	.265	.826	.959
.6	.349	1.018	1.070
.7	.435	1.162	1.163
.8	.523		
.9	.612		
1.0	.674		

Table IV. Tabulation of $\bar{\lambda}_{u1}$, $\bar{\lambda}_{s1}$, $\bar{\lambda}_{u2}$—rectangular distribution function $f_0(p)$ and trial function Eq. (58) with conducting end plates.

ϵ	$\bar{\lambda}_{u1}$	$\bar{\lambda}_{s1}$	$\bar{\lambda}_{u2}$
.2	.17	.50	.76
.3	.27	.87	.98
.4	.38		
.5	.45		
.6	.525		
.7	.566		
.8	.659		
.9	.699		
1.0	.712		

Table V. Tabulation of $\bar{\lambda}_{u1}$, $\bar{\lambda}_{s1}$, $\bar{\lambda}_{u2}$—rectangular distribution function $f_0(p)$ and trial function represented by a sum of Legendre polynomials.

$2p_0$	ϵ^+	ϵ^-	$\bar{\lambda}_{u1}$	$\bar{\lambda}_{s1}$	$\bar{\lambda}_{u2}$
.19	.09	.1	.086	.21	.534
.36	.17	.2	.111	.32	.599
.51	.23	.3	.150	.43	.618
.64	.28	.4	.193	.51	.559
.75	.32	.5	.236	.61	.633
.84	.36	.6	.272	.72	.73

Table VI. Tabulation of $\bar{\lambda}_{u1}$, $\bar{\lambda}_{s1}$, $\bar{\lambda}_{u2}$—parabolic distribution function $f_0(p)$ and trial function represented by a sum of Legendre polynomials.

Figure Captions

1. (a) End view—ion orbits pass through axis of symmetry.

   (b) Side view—disk-shaped plasma.

2. Coordinates of ion perpendicular trajectory.

3. Radial profile of ion density integrated over $z(\epsilon = .2)$.

4. Variation of $\lambda^{(j)}(\hat{\omega})$ as a function of $\hat{\omega}$ for $j = 1, 2, 3$ $(\epsilon = .2)$.

5. Trial functions $\varphi_u^{(1)}$, $\varphi_s^{(2)}$, $\varphi_u^{(2)}$ $(\epsilon = .2)$.

6. Stability boundaries in parameter space ($\bar{\lambda} = N_T/N_{\text{rigid}}$ versus ϵ)—rectangular distribution function $f_0(p)$.

(b)

(a)

Figure 1

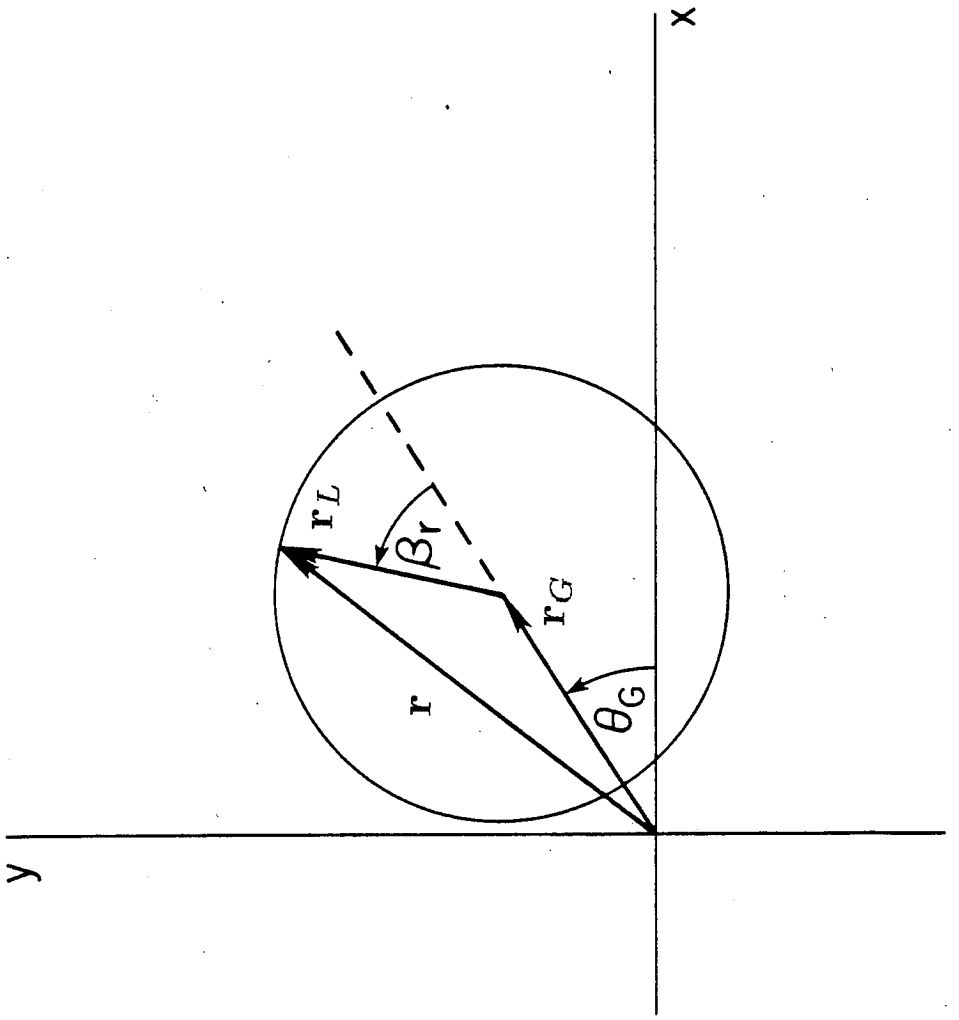

Figure 2

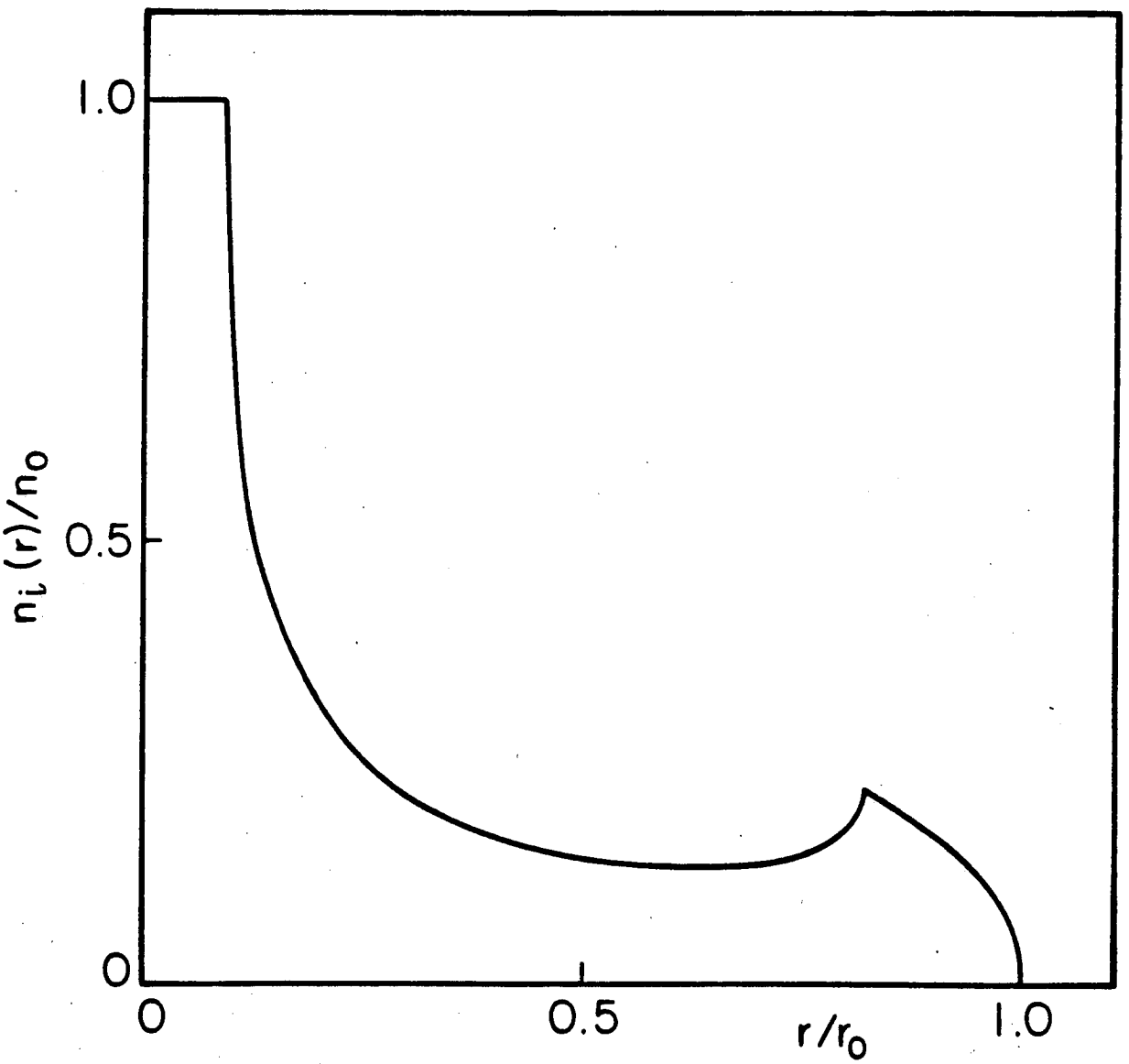

Figure 3

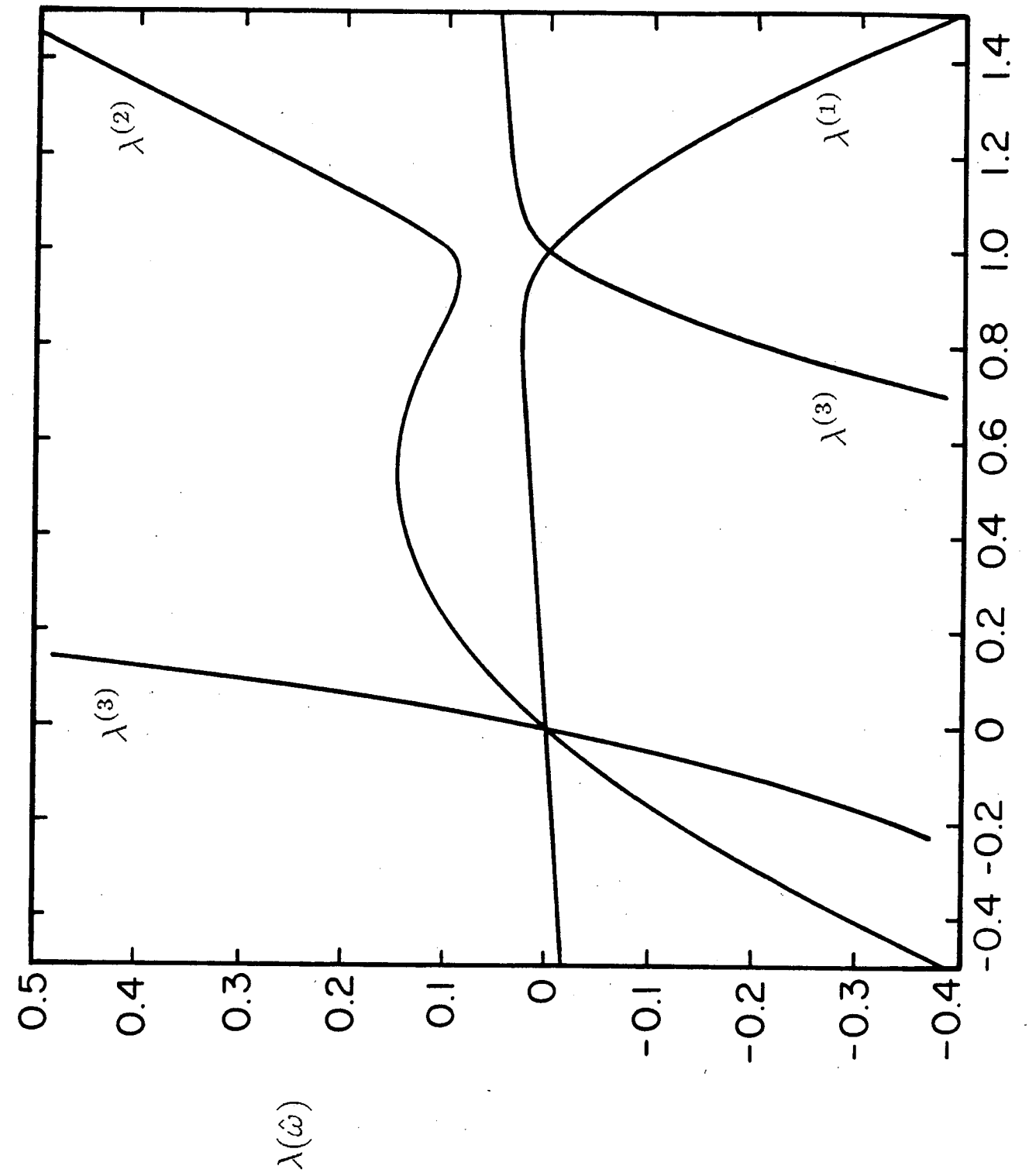
$\lambda^{(2)}$
$\lambda^{(1)}$
$\lambda^{(3)}$
$\lambda^{(3)}$
0.5
0.4
0.3
0.2
0.1
0
-0.1
-0.2
-0.3
-0.4
$\lambda(\hat{\omega})$
-0.4
-0.2
0
0.2
0.4
0.6
0.8
1.0
1.2
1.4
$\hat{\omega}$

Figure 4

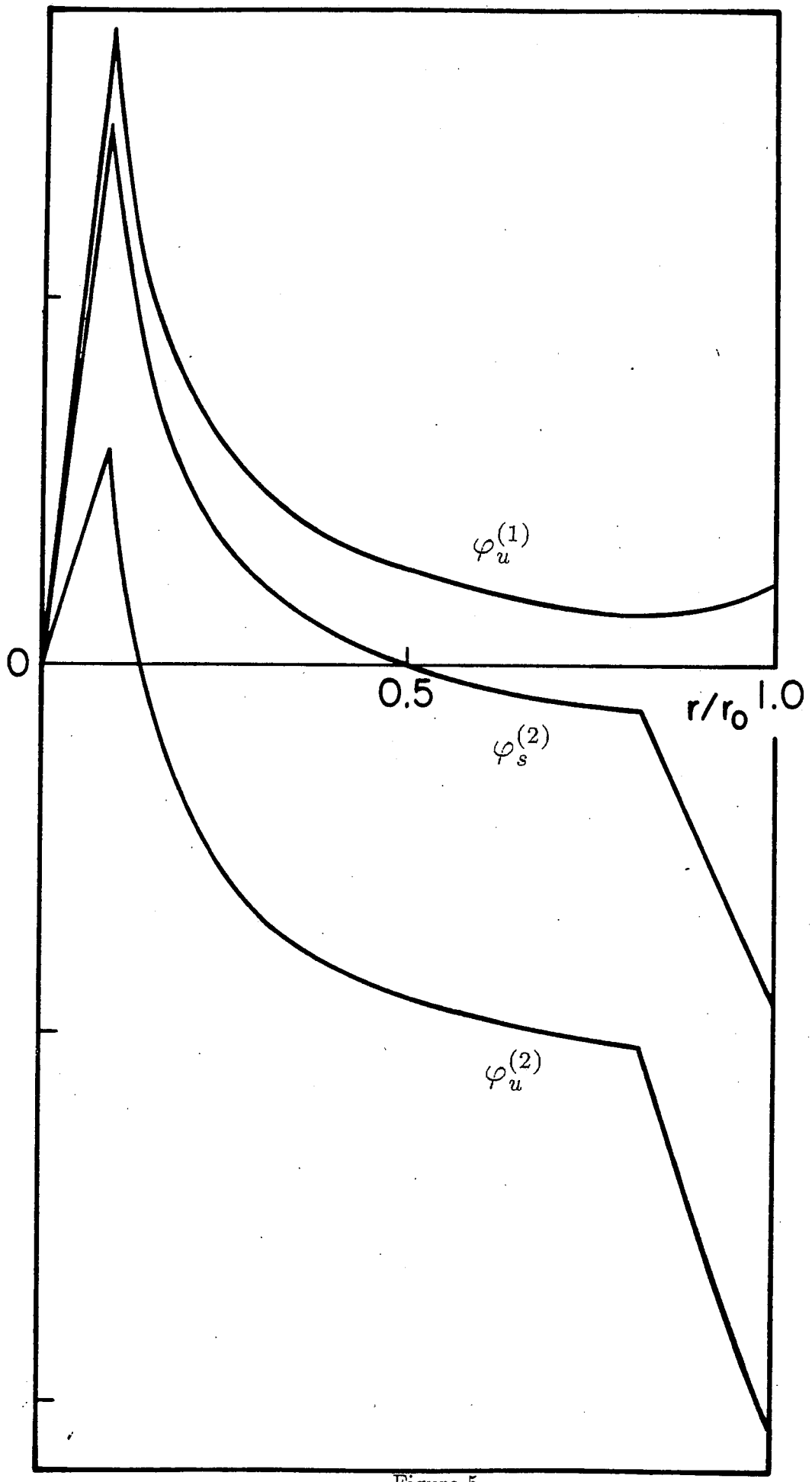

Figure 5

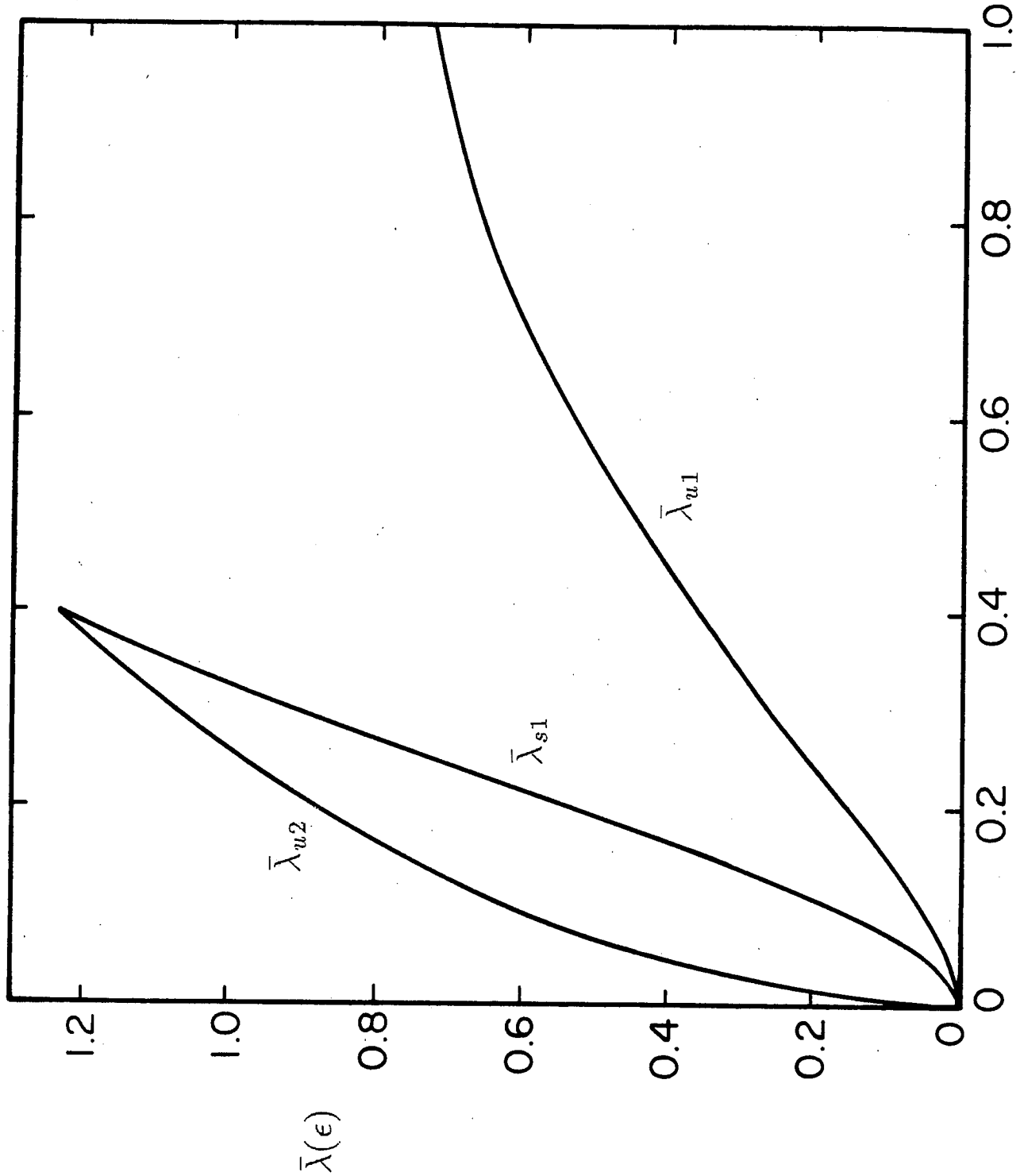
1.2
1.0
0.8
0.6
0.4
0.2
0
$\bar{\lambda}(\epsilon)$
$\bar{\lambda}_{u2}$
$\bar{\lambda}_{s1}$
$\bar{\lambda}_{u1}$
0
0.2
0.4
0.6
0.8
1.0
ϵ

Figure 6